Accepted Manuscript

Synthesis of glycerol carbonate over porous La-Zr based catalysts: The role of strong and super basic sites

Xianghai Song, Donghui Pan, Yuanfeng Wu, Pin Cheng, Ruiping Wei, Lijing Gao, Jin Zhang, Guomin Xiao

PII: S0925-8388(18)31269-6

DOI: 10.1016/j.jallcom.2018.03.392

Reference: JALCOM 45622

To appear in: *Journal of Alloys and Compounds*

Received Date: 1 September 2017

Revised Date: 28 March 2018

Accepted Date: 29 March 2018

Please cite this article as: X. Song, D. Pan, Y. Wu, P. Cheng, R. Wei, L. Gao, J. Zhang, G. Xiao, Synthesis of glycerol carbonate over porous La-Zr based catalysts: The role of strong and super basic sites, *Journal of Alloys and Compounds* (2018), doi: 10.1016/j.jallcom.2018.03.392.

Graphical Abstract

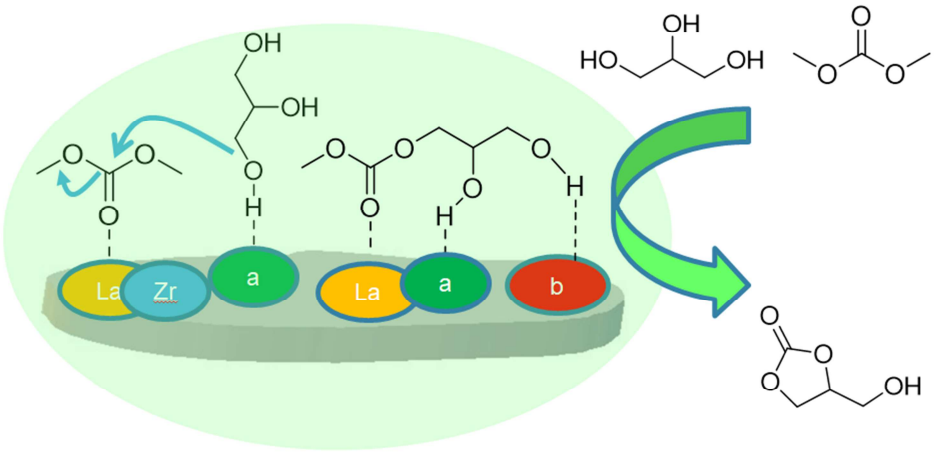

Preparation of glycerol carbonate from glycerol over KF/La-Zr solid base

Synthesis of glycerol carbonate over porous La-Zr based catalysts: The role of strong and super basic sites

Xianghai Song, Donghui Pan, Yuanfeng Wu, Pin Cheng, Ruiping Wei, Lijing Gao, Jin Zhang, Guomin Xiao*

School of Chemistry and Chemical Engineering, Southeast University, Nanjing, China

Abstract

As important glycerol derivatives, glycerol carbonate (GC) and glycidol (GD) have attracted increasing attention in recent years. In the present work, a series of new solid base catalysts were developed to catalyze the conversion of glycerol to afford GC and GD. These catalysts were prepared by loading KF on the porous La-Zr solid base catalyst and characterized using a series of methods. A large number of various basic sites were generated upon loading KF onto the La-Zr-600 support. The weak basic sites were assigned to the surface hydroxyl groups produced during the formation of LaOF, while the strong and super basic sites were related to the Lewis base produced due to the interaction between KF and the La-Zr-600 support. A glycerol conversion of 91.77% and a GC selectivity of 99% were obtained over 0.3KF/La-Zr, which displayed the best catalytic performance under the optimal reaction conditions. The excellent activity of these catalysts was attributed to the presence of the strong and super basic sites, which favor the transesterification of glycerol with dimethyl carbonate. The production of GD from GC decarbonylation was unfeasible at low temperature using the newly developed catalysts. A plausible reaction mechanism has been proposed based on the experimental results and characterization.

Keywords: Glycerol, Glycidol, Glycerol carbonate, KF/La-Zr, Basic sites

1. Introduction

The biodiesel industry has rapidly increased worldwide over the last decades in an effort to reduce our dependence on fossil fuels. However, the expansion in biodiesel production has generated huge amounts of glycerol as a by-product, which has seriously hampered the development of the biodiesel industry. The conversion of glycerol to high value-added products is a perfect way to utilize glycerol by-products formed during production of biodiesels and has attracted a considerable amount of attention [1-3]. Several conversion processes have been reported for the synthesis of valuable glycerol derivatives [4, 5]. Among the various derivatives of glycerol, glycerol carbonate (GC) and glycidol (GD) are of great importance due to their wide ranging applications. GC can be used for the manufacturing of coatings, biolubricants, polycarbonates, polyesters, and polyurethanes due to its low flammability, low toxicity, and biodegradability [6-8].

It can also be used as a solvent due to its high boiling point [9]. On the other hand, GD is utilized as a stabilizer, plastic modifier, fire retardant, and surfactant [10]. In addition, GD can also be used as a raw material for the preparation of polyglycerol, glycidyl ethers, and propanediols [11-13].

Over the past few years, extensive research has been carried out on the catalytic conversion of glycerol to GC. For example, the transesterification of glycerol with dimethyl carbonate (DMC) has been widely reported in the production of GC [14-16]. However, only a few studies on the synthesis of GD from glycerol have been reported to date. Malkemus et al. first patented the production of GD from GC using a metal salt as a homogeneous catalyst, achieving GD yields of 80%–90% at high temperature (175–225 ^{o}C) and reduced pressure [17]. Later, zeolite-A was used as a heterogeneous catalyst for the patented synthesis of GD from GC at 3.5 kPa and 183 ^{o}C [18]. In the presence of a solvent and the absence of active hydrogen, anhydrous Na_2SO_4 has been shown to be effective for the preparation of GD at 200 ^{o}C and 2.7 kPa [19]. Moreover, an ionic liquid has also been found to be useful in the production of GD from GC [20]. Bolívar-Diaz et al. selectively transformed GC into GD under mild conditions using a ZSM-5 zeolite catalyst and a zinc oxide-supported nanoscale cobalt oxide catalyst [21].

Accordingly, to prepare GD directly from glycerol via the decarbonylation of GC is of great interest and thus has recently attracted a great deal of research attention. Kelkar et al. reported the first preparation of GD from glycerol with high GD selectivity (78%) using tetramethylammonium hydroxide as a catalyst at 80 ^{o}C [22]. Later, they found that a 1,4-diazabicyclo[2.2.2]octane based ionic liquid was also highly active in the decarbonylation of GC obtained from the transesterification of glycerol to give GD [23]. A Mg/Zr/Sr mixed oxide was proven to be active for the production of GD and achieved a GD yield of 40% [24]. In addition, a KF/sepiolite catalyst was also developed by Algoufi et al., which was used for the production of GD from glycerol [25]. To date, the research in this area is still limited and thus, further study is needed.

The preparation of GD directly from glycerol via the decarbonylation of GC involves two steps as shown in Scheme 1: (1) The transesterification of glycerol with DMC to produce GC and (2) the decarbonylation of GC to yield GD. The transesterification of glycerol can be easily achieved in the presence of a basic catalyst [26, 27]. However, the decarbonylation of GC requires special conditions, such as high temperature [17, 20], reduced pressure [18] or the requirement a use of solvent [28].

Some studies on the preparation of GD at low temperature have been reported [22-25]. In this work, we aimed to develop a new type of catalyst comprised of various basic sites, which exhibited both excellent activity for glycerol transesterification and good selectivity towards GD. Various catalysts, including metal oxides and alkaline metal salts were investigated. The results

indicated that loading La-Zr with KF resulted in the best catalytic performance and the highest GD selectivity. However, analysis of the product showed that GC was the only product of the reaction. GD that was formed was derived from the decomposition of GC in the injection port of the gas chromatograph due to its high temperature. It seems that the preparation of GD at low temperature is not possible.

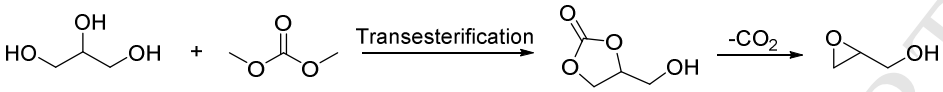

Scheme 1 Preparation of GD from glycerol and dimethyl carbonate.

2. Experimental section

2.1 Materials

$La(NO_3)_3 \cdot 6H_2O$ (AR), $Zr(NO_4)_4 \cdot 5H_2O$ (AR), CaO (AR) were purchased from Sinopharm Chemical Reagent Co., Ltd. PEG-PPG-PEG Pluronic® P-123 (Mn~5800) was purchased from Sigma-Aldrich. SrO (AR), K_2CO_3 (AR) and KF anhydrous (AR) were obtained from Aladdin Industrial Corporation, Shanghai, China. Glycerol (AR), dimethyl carbonate (DMC) (AR) were obtained from Sinopharm Chemical Reagent Co., Ltd., Shanghai, China. Glycidol (96%) was purchased from Heowns Biochem Technologies Co., Ltd. Glycerol carbonate (96.6%) was supplied by Accela ChemBio Co. Ltd.

2.2 Catalyst preparation

2.2.1 Preparation of porous La-Zr-600

The porous La-Zr mixed oxides were prepared by a co-precipitation method with P123 as model template. In the experiment, P123 (2.41 g) was dissolved in 160 mL of deionized water and stirred for another 30 minutes after dissolution. Then the system was acidified with 1 M HNO_3 to PH=1-2. $La(NO_3)_3 \cdot 6H_2O$ (6.93 g), $Zr(NO_4)_4 \cdot 5H_2O$ (6.87 g) were added to the solution mentioned above under vigorous stirring for 3 h. Subsequently, the solution was basified with K_2CO_3 (40 wt.%) to PH=9-10. The obtained mixture was kept at 40 ^oC for 12 h, and then hydrothermal treated at 180 ^oC for 24 h. The resulted solid was separated by centrifugation and washed with a large amount of deionized water to PH=7. Finally the obtained solid was dried at 120 ^oC for 12 h and then annealed at 600 ^oC for 5 h. The resulted catalyst was marked as La-Zr-600.

2.2.2 Preparation of La-Zr-600 supported KF

La-Zr-600 supported KF was prepared by wet impregnation. Typically, calculated amount of anhydrous KF (0.30 g), La-Zr-600 (1.02 g) and 20 mL deionized water were placed into a 100 mL flask. The resulted mixture was stirred at room temperature for 12 h, after which the water was removed by evaporation at reduced pressure. After drying at 100 ^oC for 12 h, the obtained sample was annealed at 500 ^oC for 5 h. The resulted catalyst was denoted as xKF/La-Zr, where x

represented the mass ratio of KF to La-Zr-600.

2.3 Catalyst characterization

X-ray diffraction (XRD) patterns of the catalysts were obtained using a Rigaku D/max-A diffractometer. The scanning range (2θ) was within 5-80°, at a scanning rate of 20° min^{-1} and a step function of 0.02.

N_2 adsorption–desorption isotherms were performed on a Beishide 3H-2000 analyser by static N_2 physisorption at -196 ^oC. The surface area of the prepared catalysts was calculated based on multipoint Brunauer–Emmett–Teller (BET) method. Pore size and pore volume was calculated from desorption branches of the isotherms through Barrett–Joyner–Halenda (BJH) method.

The surface functional groups were determined by fourier transform infrared spectrometer (FT-IR) on a Nicolet 5700 spectrometer, in the wavenumber range of 400-4000 cm^{-1} with KBr as a reference for the measurements.

Thermogravimetric (TG) analysis was conducted using a TG 209 F3 Tarsus instrument. In a typical procedure, about 5 mg catalyst was placed into an aluminum pan which was then treated on the instrument under air atmosphere from 50 to 800 ◦C at a heating rate of 10 ◦C per minute.

Temperature programmed desorption (CO_2-TPD) was performed to determine the basicity of the catalyst. The moisture and other adsorbed gases were removed by pretreating the sample at 300 ^oC for 1 h in a flow of He (30 mL min^{-1}). Subsequently, the sample was cooled down to 50 °C, and exposed to pure CO_2 for 30 minutes. The physically adsorbed CO_2 was excluded by purging the sample with He flow (30 mL min^{-1}) for 1 h. Thereafter, the sample was heated to 700 ^oC at a rate of 10 ^oC min^{-1} and the desorbed CO_2 was detected by a thermal conductivity detector.

The TG-MS was carried out on a 409PC thermal analyzer (Netzsch, Germany) coupled with a QMS403C instrument (Netzsch, Germany). In the experiment, 10 mg sample was heated at 10 °C min^{-1} from 40 to 600 °C in argon. Mass scanning was performed in the range m/z 2-200.

X-ray photoelectron spectroscopy (XPS) was measured on a Thermo Fisher Scientific ESCALAB 250Xi X-ray photoelectron spectrometer, using nonmonochromatized Mg Kα radiation (1253.6 eV) as the X-ray source. The precision of the binding energy values were within 0.1 eV. The binding energy values were calibrated by referencing the C 1s signal (285.0 eV).

2.4. Catalytic activity test

The preparation of GD from glycerol and DMC was performed in a 50 mL round bottomed flask equipped with a thermometer, a magnetic stirring bar and a rectifying column connected to a liquid dividing head. In a typical experiment, 50 mmol (4.62 g) of glycerol and 100 mmol (9.05 g) of DMC were placed into the flask, followed by 0.14 g (3 wt.%) of catalyst. Subsequently, the reaction system was heated to the desired temperature for a designed time. During the reaction, the

byproduct methanol was separated in suit to facilitate the reaction. After the reaction was completed, the catalyst was separated from the reaction system by centrifugation. The product was analyzed using a gas chromatograph (GC-6890, China), equipped with a flame ionization detector and a capillary column (SE-30, 30 m × 0.25 mm). 2-Butoxy ethanol was added to the product as an internal standard for the quantification analysis.

3. Results and discussion

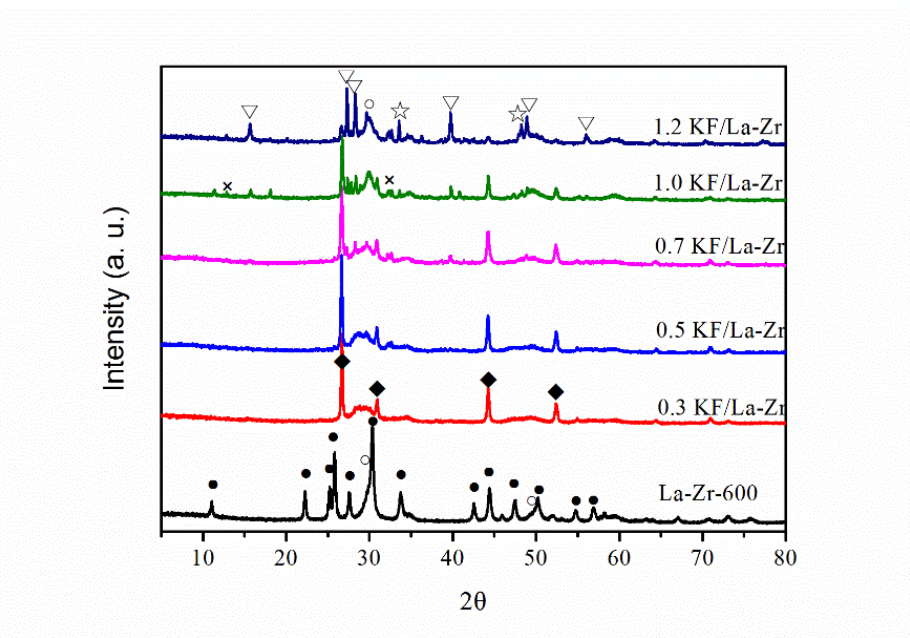

Fig. 1 XRD patterns of various catalysts. ● $La_2O_2CO_3$, ○ ZrO_2, ◆ LaOF, ☆ KF, ▽ $KLaF_4$, × $K_2CO_3(H_2O)_{1.5}$.

3.1 Characterization of catalysts

3.1.1 XRD characterization

The XRD patterns of La-Zr-600 and La-Zr-600 loaded with different amounts of KF are presented in Fig. 1. La-Zr-600 exhibits the typical characteristic peaks of $La_2O_2CO_3$ (JCPDS Card No. 84-1963) and the small characteristic peaks of ZrO_2 (JCPDS Card No. 49-1642). The good dispersibility of ZrO_2 in the catalyst may account for its small peaks when compared with $La_2O_2CO_3$. After loading with 30 wt.% KF, the peaks for $La_2O_2CO_3$ are completely replaced by the peaks of LaOF (JCPDS Card No. 44-0121) in 0.3KF/La-Zr, indicating the product of the reaction between $La_2O_2CO_3$ and KF was LaOF (Scheme 2) [29]. The new LaOF species may be responsible for the high activity and GD selectivity. However, the peaks for ZrO_2 were almost unchanged, which means ZrO_2 may not react with KF. New characteristic diffraction peaks for $KLaF_4$ (JCPDS Card No. 75-1927) are observed in the 0.7KF/La-Zr catalyst. Besides, the intensity of the diffraction peaks for $KLaF_4$ increases upon increasing the loading amount of KF and the

peaks for LaOF almost disappear in 1.2KF/La-Zr, revealing LaOF can further react with KF to form $KLaF_4$ (Scheme 2). Moreover, the diffraction peaks for KF appear in 1.0KF/La-Zr and increase upon increasing the loading amount of KF. This means that to some extent, KF was dispersed in the catalyst and interacts with the support, and beyond this extent the excess KF will agglomerate on the surface of the support. The possible reaction between the La-Zr-600 support and KF may occur as follows:

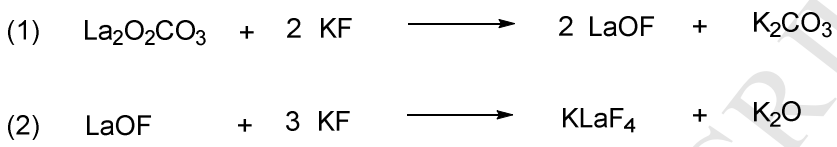

Scheme 2 Possible reaction formula between KF and La-Zr-600.

The existence of K_2CO_3 was confirmed by the diffraction peaks observed in the XRD patterns (Scheme 2). The formation of LaOF from the reaction between La_2O_3 (or $La_2O_2CO_3$) and KF has been reported previously [30, 31]. However, K_2O that was found in the second step was not detected and this may be due to the high dispersion degree of K_2O in the catalyst. The presence of $KCaF_3$ and K_2O on CaO loaded with KF may serve as a reference for the second reaction [32]. The strong base K_2O may also account for the high activity of the La-Zr-600 supported KF.

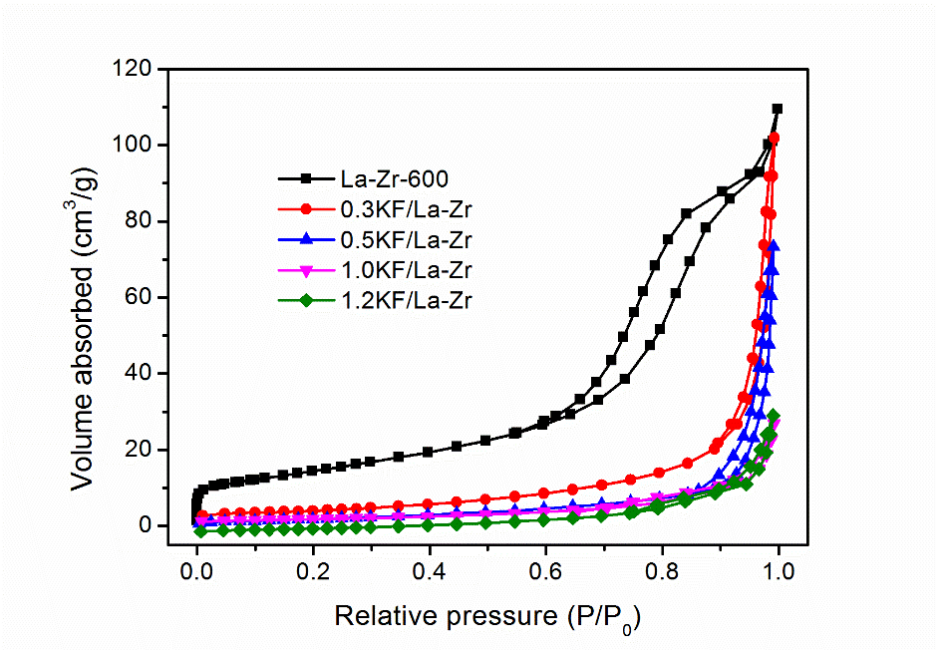

Fig. 2 N_2 adsorption-desorption isotherms of various La-Zr catalysts.

3.1.2 Morphologies characterization

Table 1 Textural parameters of the prepared catalysts

Catalyst	BET surface area (m^2/g)	Pore size (nm)	Pore volume (cm^3/g)
La-Zr-600	52.21	12.97	0.17
0.3KF/La-Zr	14.49	43.54	0.16
0.5KF/La-Zr	10.41	44.22	0.12
1.0KF/La-Zr	6.30	26.34	0.04
1.2KF/La-Zr	7.31	26.82	0.05

The morphologies of the as-prepared catalysts were characterized using N_2 adsorption-desorption isotherms and the results displayed in Fig. 2. Clearly, La-Zr-600 exhibits a type IV isotherm with a hysteresis loop at P/P_0 = 0.59–0.99, indicating the presence of mesopores [33]. In addition, a sharp increase in the N_2 adsorption amount was observed at low pressure, implying the existence of micropores [34]. The formation of mesopores and micropores was attributed to the removal of the soft template (P_{123}). The surface area of the catalysts decreases sharply upon loading with KF from 52.21 m^2/g for La-Zr-600 to 6.30 m^2/g for 1.0KF/La-Zr, as shown in Table 1. The decreased surface area may be related to the blocking of the pores in the catalysts by the loaded KF. In addition, the pore volume decreases upon increasing the loading amount of KF, which was in agreement with the change in the surface area. However, the pore size of the catalysts first increased and then decreased upon increasing the loading amount of KF. Considering the pores are blocked by KF, the larger pore size can be attributed to the void space between the catalyst particles [35, 36]. Moreover, KF on the La-Zr-600 surface began to agglomerate when the content of KF reached a particular amount, as described in the XRD analysis. This agglomeration may account for the reduced pore size of the catalysts upon increasing the amount of KF.

3.1.3 FT-IR characterization

The surface species of the as-prepared catalysts were also investigated using FT-IR spectroscopy and the results are shown in Fig. 3. The absorption bands within 700–1500 cm^{-1} are attributed to various vibration modes of CO_3^{2-} [32]. The bands around 873, 1089 and 1398 cm^{-1} are assigned to the characteristic bands of $La_2O_2CO_3$ [37-39]. All the La-Zr-600 catalysts display an absorption band at around 1464 cm^{-1} upon the addition of KF. The new band may be related to the C-O stretching mode of K_2CO_3, which was produced due to the reaction of KF and $La_2O_2CO_3$, as shown in Scheme 2 [30]. The bands at 3000–3500 and 1663 cm^{-1} are associated with the O-H stretching mode and O-H bending vibration of the hydroxyl groups, respectively [26]. Moreover,

the peak area of these bands increases upon increasing the loading amount of KF, which was in accordance with the deliquescent properties of KF. Besides, a small absorption band at 2349 cm^{-1}, which was assigned to the adsorbed CO_2, was also observed and indicated the existence of strong basic sites. The FT-IR results match well with the XRD analysis.

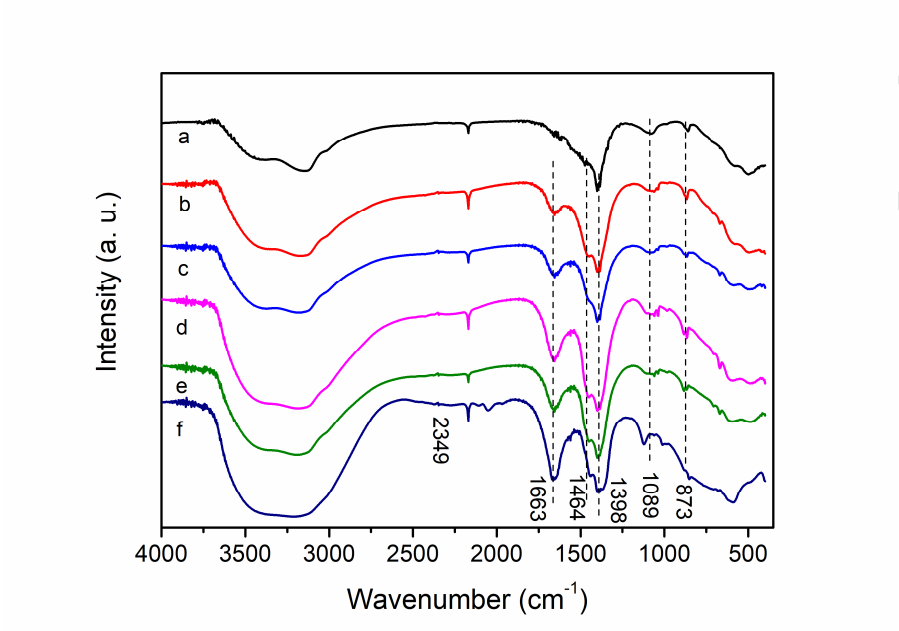

Fig. 3 FT-IR spectra of (a) La-Zr-600, (b) 0.3KF/La-Zr, (c) 0.5KF/La-Zr, (d) 0.7KF/La-Zr, (e) 1.0KF/La-Zr, (f) 1.2KF/La-Zr.

3.1.4 TG characterization

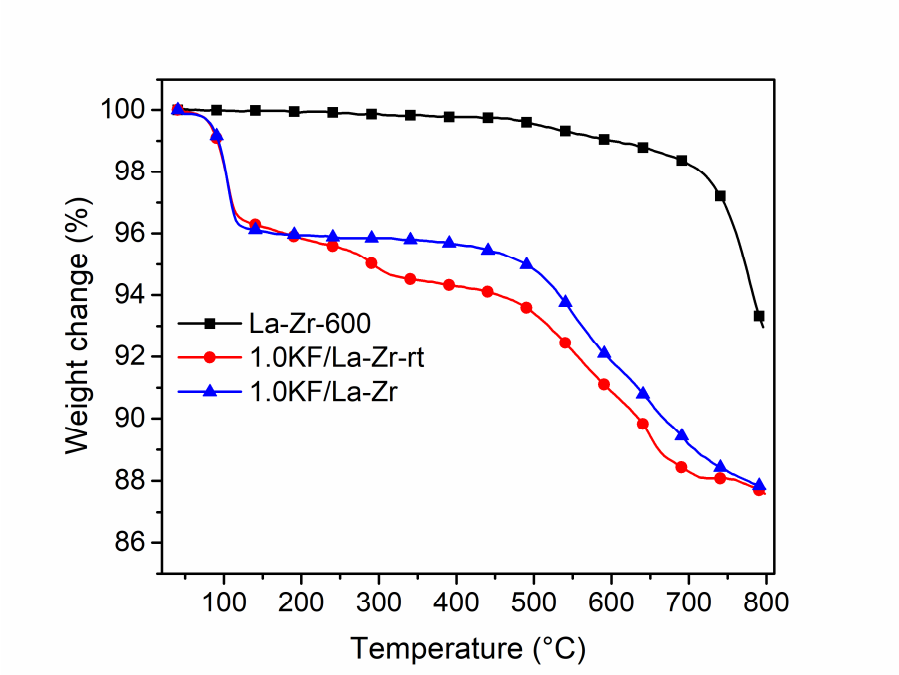

Fig. 4 TG curves of La-Zr-600, 1.0KF/La-Zr-rt (1.0KF/La-Zr without calcination), 1.0KF/La-Zr.

The thermal behavior of La-Zr-600 and La-Zr-600 loaded with KF was investigated by thermogravimetric analysis and the results are displayed in Fig. 4. Obviously, La-Zr-600 was quite stable before 480 ^{o}C and there was a slight weight loss of 0.91% between 480 and 600 ^{o}C. Considering the sample was treated at 600 ^{o}C, the weight loss within 480–600 ^{o}C may be attributed to the decomposition of $La_2(CO_3)_3$ formed in the cooling process of the sample due to the absorption of CO_2 in the air [39]. The marked decrease in weight above 700 ^{o}C should be ascribed to the decomposition of $La_2O_2CO_3$ and the structural carbonate [30, 40]. thermogravimetric analysis–mass spectroscopy was performed to verify the products of the decomposition process, as shown in Fig S1. Clearly, H_2O and CO_2 were detected at around 480 ^{o}C and a large amount of CO_2 is detected above 700 ^{o}C. Thus, the products of the catalyst decomposition were CO_2, La_2O_3, and a small amount of water. Both 1.0KF/La-Zr and 1.0KF/La-Zr-rt present a weight loss of about 3.8% below 100 ^{o}C, which was attributed to the adsorbed water due to the facile deliquescence of KF. When compared with 1.0KF/La-Zr, 1.0KF/La-Zr-rt exhibits a weight loss of 1.12% between 200–300 ^{o}C, indicating the interaction of KF and La-Zr-600. Similarly, a decrease in weight at high temperature was also observed in these two samples, while the beginning temperature shifted to 480 ^{o}C, which was about 220 ^{o}C lower than that of La-Zr-600. The lower decomposition temperature may be related to the formation of easily decomposed species, as indicated by XRD analysis. Besides, the interaction between KF and the support may also lead to the decreased decomposition temperature.

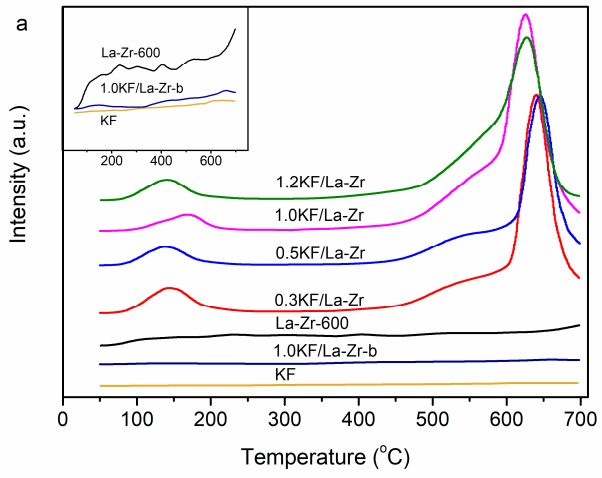

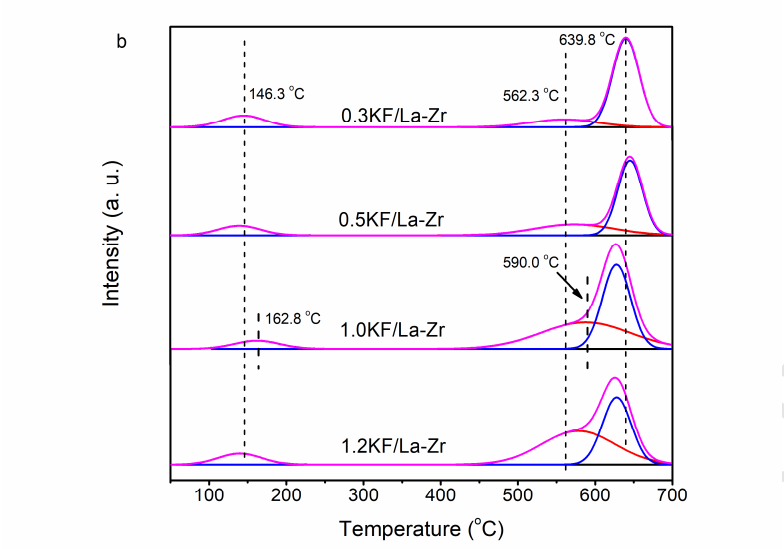

Fig. 5 CO_2-TPD profiles of the prepared KF/La-Zr catalysts.

Table 2 CO_2-TPD data for various KF/La-Zr catalysts

Catalyst	Weak base		strong base		Super base		TBA[c]
	T[a](°C)	Area[b]	T[a] (°C)	Area[b]	T[a] (°C)	Area[b]	
0.3KF/La-Zr	146.3	605.36	562.3	626.63	639.8	2834.82	4066.81
0.5KF/La-Zr	139.9	450.27	575.9	965.76	644.5	2048.26	3464.29
1.0KF/La-Zr	162.8	394.87	590.0	2513.18	627.3	2537.58	5445.63
1.2KF/La-Zr	141.1	506.03	575.3	2579.41	626.8	2019.84	5105.28

[a] Temperature of desorption peak. [b] CO_2 desorption peak area of various basic sites. [c] Total CO_2 desorption peak area of various basic sites.

3.1.5 CO_2-TPD characterization

The basicity of the catalyst is responsible for the transesterification of glycerol and the subsequent decarboxylation of GC to give GD. Hence, CO_2-TPD was performed to investigate the basicity of the as-prepared KF/La-Zr catalysts (Fig. 5)., The magnified profiles of KF and La-Zr-600 are displayed in Fig. 5a to fully understand the basic properties of the two samples due to their poor signals when compared with the KF/La-Zr catalysts. Clearly, almost no CO_2 desorption peak was observed for pure KF, indicating the absence of basicity in the pure KF sample. The La-Zr-600 sample exhibits evident multi-desorption peaks of CO_2 at around 158, 231, 405, and 528 °C, implying the presence of weak, moderate and strong basic sites in the sample. There are few basic sites on the surface of La_2O_3 or $La_2O_2CO_3$, thus the basicity of La-Zr-600 may originate from the La-Zr solid solution [40]. According to the TGA, after loading with KF the catalyst decomposes

obviously within 480–700 ^{o}C. Thus, a blank experiment (1.0KF/La-Zr-b: 1.0KF/La-Zr without CO_2 adsorption) was performed to investigate the influence of the catalyst decomposition process on the CO_2-TPD profiles. Though 1.0KF/La-Zr-b (blank experiment) presents desorption peaks in the zoomed in profile, these peaks can be ignored when compared with that of 1.0KF/La-Zr after CO_2 adsorption. Hence the effect of the catalyst decomposition process was almost negligible. After loading with KF, the KF/La-Zr catalysts present intense CO_2 desorption peaks (Fig. 5a), suggesting the strong interaction between KF and the La-Zr-600 support. These basic sites may originate from the new species formed due to the reaction between KF and La-Zr-600. Besides, the interaction between KF and the La-Zr-600 support may also be responsible for these basic sites.

Deconvolution of the CO_2-TPD profiles was performed to further understand the basic properties of the catalysts (Fig. 5b). Clearly, all the samples present three peaks at around 150, 560 and 630 ^{o}C, which are attributed to desorption of CO_2 from the weak, strong and super basic sites, respectively [30]. The weak basic sites are associated with the Brønsted base sites, while the strong and super basic sites should be related to the Lewis base sites. According to the literature, the weak basic sites are attributed to the surface hydroxyl groups, which are produced during the formation of LaOF [29], as demonstrated by XRD and IR analyses. In addition, LaOF may also be responsible for the basic sites in the catalyst [31]. The electronegativity of F^- is higher than lattice oxygen (O^{2-}), which results in the pull of the negative charge of lattice oxygen towards the F^- ion and the formation of strong basic sites [29, 33]. Thus, the strong basic sites should be derived from the interaction between the highly dispersed KF and the La-Zr-600 support. In addition, the produced K_2O may also account for the strong basic sites, as depicted in Scheme 2. The amount of alkaline and temperature of the desorption peaks observed for the various catalysts are summarized in Table 2. The amount of strong basic sites increases upon increasing the KF loading to 50% (1.0KF/La-Zr) with a shift in the desorption peak to higher temperature. A further increase in the KF loading leads to a decrease in the desorption temperature. This phenomenon may be due to the complicated interaction between the KF and the support. Considering all the catalysts loaded with KF exhibit a high glycerol conversion when compared with La-Zr-600, the strong and super basic sites should play key roles in the transesterification of glycerol to afford GC and GD.

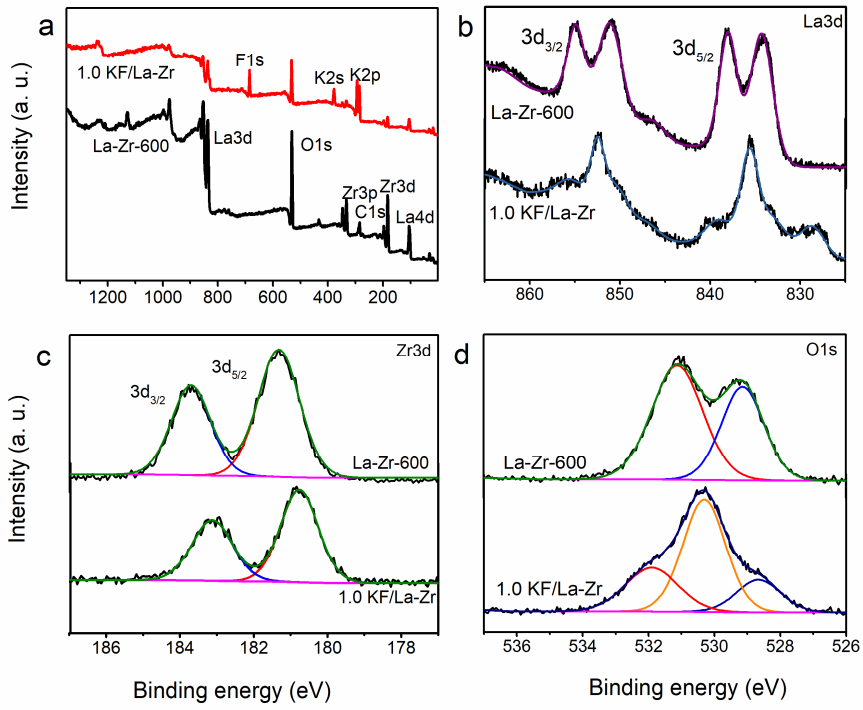

Fig. 6 XPS spectra of La-Zr-600 and 1.0KF/ La-Zr, (a) full spectra, (b) La3d, (c) Zr3d, (d) O1s.

3.1.6 XPS characterization

XPS characterization was employed to gain further insight into the chemical state of the species present on the surface of the catalysts (Fig. 6). The characteristic peaks for the elements La, Zr, O and C were observed in La-Zr-600, which was in good agreement with the XRD results. After loading with KF, the signals for K and F were detected in 1.0KF/La-Zr, implying KF was successfully loaded onto the support (Fig. 6a). The La 3d spectra of La-Zr-600 presents two peaks at 855.0 and 838.1 eV, which were assigned to the characteristic $3d_{3/2}$ and $3d_{5/2}$ levels of La^{3+}, respectively (Fig. 6b) [41, 42]. The doublet structures of these two peaks are attributed to multiplet splitting [43]. However, the La 3d spectrum observed for 1.0KF/La-Zr was completely different from that observed for La-Zr-600. Two main peaks are observed at 852.4 and 835.6 eV, which were accompanied by some small peaks at 856.3, 839.5 and 828.7 eV, in the La 3d spectrum of 1.0KF/La-Zr. The complicated peak shape of La 3d may be related to the co-existence of various La species, such as La_2O_3, $La_2O_2CO_3$, LaOF, and KLaF, which were in accordance with the XRD results. The Zr 3d peaks observed at 183.7 and 181.3 eV in La-Zr-600 (Fig. 6c) are assigned to the

$3d_{3/2}$ and $3d_{5/2}$ levels of Zr^{4+}, and are derived from the spin–orbit splitting [44]. In comparison to La-Zr-600, the Zr 3d spectrum of 1.0KF/La-Zr was almost unchanged with only a little shift to the lower binding energy by 0.5 eV. The shift in the binding energy may be associated with the interaction between ZrO_2 (or La-Zr solid solution) and KF. The O1s spectrum for La-Zr-600 can be roughly divided into two peaks (Fig. 6d). The peak at around 529.1 eV was attributed to the lattice oxygen (O^{2-}) of La_2O_3 and ZrO_2 [39, 44, 45], while the peak centered at 531.1 eV was assigned to the CO_3^{2-} in $La_2O_2CO_3$ [46, 47]. After being treated with KF, 1.0KF/ La-Zr presents an intense peak at 530.3 eV, which was due to the generation of a new environment around the surface oxygen atoms, which may be related to the new LaOF species, as depicted in the XRD analysis [29]. According to the characterization mentioned above, it seems that the interaction between KF and La-Zr-600 mainly occurs on the La species.

3.2 Catalytic activities

3.2.1 Catalyst screening

Table 3 Catalytic activity of various catalysts for the production of GD and GC [a]

Catalyst	Gly. conv. (%)	GD Sel. (%)	GC Sel. (%)[d]	GC yield (%) [d]
KF	19.93	26.70	73.30	14.61
CaO	81.85	7.09	92.91	76.05
SrO	50.64	4.36	95.64	48.44
La_2O_3 [b]	70.00	22.00	77.00	53.90
La-Zr-600	15.97	0	100.00	15.97
KF+La-Zr-600 [c]	38.43	31.09	68.91	26.48
0.3KF/La-Zr	91.77	46.89	53.11	48.74

[a] Reaction conditions: Glycerol 50 mmol, DMC 100 mmol, catalyst 3 wt.%, 80 ^oC, 60 min. [b] 120 ^oC, DMF as solvent, 90 min, Reference [28]. [c] A mixture of 0.03 g KF and 0.10 g La-Zr-600. [d] The yield and selectivity are calculated based on gas chromatography.

According to the literature, basic catalysts are active for the transesterification of glycerol to afford GC, and strong bases and alkaline metal salts are beneficial for the decarbonylation of GC to give GD. Thus, various catalysts have been utilized to catalyze the production of GD from glycerol, which are presented in Table 3. Clearly, KF itself displays poor glycerol conversion and GD selectivity. The glycerol conversion of CaO and SrO is moderate, but the selectivity towards GD is low. According to the literature, La_2O_3 presents a glycerol conversion of 70% and GD selectivity

of 22%, while the reaction needed to be performed at 120 ^{o}C and in the presence of DMF. It has been reported that the presence of ZrO_2 could improve the basicity of La_2O_3 [38]. However, when La-Zr-600 was used as the catalyst, both the glycerol conversion and GD selectivity were poor, which may be attributed to the low reaction temperature (80 ^{o}C). The combination of KF and La-Zr-600 exhibits a glycerol conversion of 38.43% and GD selectivity of 31.09%, indicating the synergistic effect between KF and La-Zr-600. Moreover, when KF was loaded onto La-Zr-600, the conversion of glycerol increased markedly to 91.77% and the selectivity towards GD also increased to 46.89%. According to the CO_2-TPD results, extensive strong and super basic sites are generated on La-Zr-600 after being loaded with KF. Thus, the better glycerol conversion and high selectivity of GD should be related to the strong and super basic sites on the surface of 0.3KF/La-Zr as a result of the interaction of KF and the La-Zr-600 support.

3.2.2 Identification of product

Considering many of the literature methods used to produce GD require special conditions (high temperature and reduced pressure), the appearance of GD at 80 ^{o}C under atmosphere pressure seems to be unbelievable. Thus, ^{1}H- and ^{13}C-NMR spectroscopy was performed to confirm that GD was indeed produced during the reaction, After removing DMC and methanol by evaporation, the product of 0.3KF/La-Zr was isolated and subjected to ^{1}H-NMR and ^{13}C-NMR analysis (Fig. 7a and b). The ^{1}H-NMR spectrum shows that the product was almost pure GC; the peaks corresponding to GD at δ = 2-3 were absent (Fig. S2). Furthermore, the ^{13}C-NMR spectrum of the product presented an intense peak at δ =155.64, which was the characteristic peak of the carbonyl; again the peaks corresponding to GD were not observed (Fig. S3). These results show that no GD is produced in the reaction. To further confirm the result, the reaction process was monitored by ^{1}H-NMR spectroscopy to determine the reaction pathway (Fig. 7c). The peak intensity of glycerol (Fig. S4) decreased as the reaction proceeded and the peak intensity of GC increased as the reaction time progressed, while no peaks for GD were observed during this process, suggesting no GD was produced during the reaction. In addition, FT-IR spectroscopy also shows the product produced was GC and not GD (Fig. 7d), as indicated by the sharp peak corresponding to the carbonyl group at around 1750 cm^{-1}. Moreover, no GD was detected by ^{1}H-NMR spectroscopy even when the temperature was increased to 100 ^{o}C. According to the literature, the preparation of

GD was conventionally carried out at high temperature (175–200 ^{o}C) [17-19]. The GD detected on the gas chromatograph was a result of the decomposition of GC due to the high temperature of the injection port (270 ^{o}C). Thus, the product of the reaction over 0.3kF/La-Zr was GC and the synthesis of GD at low temperature seems to be impossible over this catalyst.

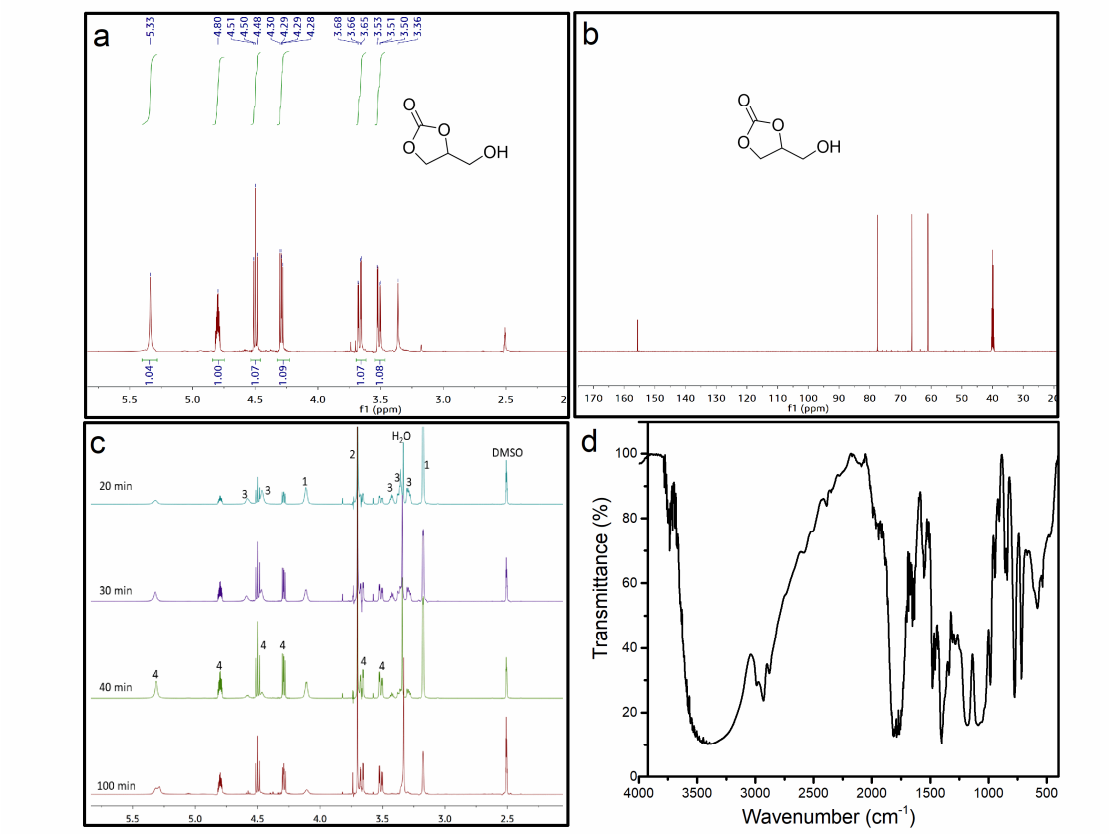

Fig. 7 (a) ^{1}H-NMR of the product over 0.3kF/La-Zr, (600 MHz, DMSO-D6) δ = 5.33 (s, 1H), δ = 4.78-4.82 (m, 1H), δ = 4.50 (t, 1H), δ = 4.28-4.30 (m, 1H), δ = 3.65-3.68 (dd, 1H), δ = 3.50-3.53 (dd, 1H). (b) ^{13}C-NMR δ = 155.64, 77.49, 66.33, 61.05. (c) ^{1}H-NMR of the reaction at different time, the number 1, 2, 3 and 4 represents methanol, DMC, glycerol and GC, respectively. (d) FT-IR of the product.

3.2.3 Effects of reaction parameters

Table 4 Effects of reaction parameters

Catalyst	Catalyst loading (%)	Time (min)	Temperature (^{o}C)	Glycerol Conv. (%)	GC Sel. (%)
0.1KF/La-Zr	3	90	80	85.22	>99
0.3KF/La-Zr	3	90	80	90.70	>99
0.5KF/La-Zr	3	90	80	91.21	>99
0.7KF/La-Zr	3	90	80	91.44	>99
0.3KF/La-Zr	0.5	90	80	74.43	>99
0.3KF/La-Zr	1	90	80	91.51	>99
0.3KF/La-Zr	5	90	80	92.61	>99
0.3KF/La-Zr	1	90	70	36.30	>99
0.3KF/La-Zr	1	90	90	91.42	>99
0.3KF/La-Zr	1	20	80	47.55	>99
0.3KF/La-Zr	1	40	80	73.52	>99
0.3KF/La-Zr	1	60	80	91.77	>99

The La-Zr-600 supported KF catalysts were further studied to obtain the optimum reaction parameters and the results presented in Table 4. Clearly, the KF loading amount has a significant effect on the glycerol conversion, which increases upon increasing the loading amount of KF from 85.22% (0.1KF/La-Zr) to 90.70% (0.3KF/La-Zr). Further increasing the KF loading amount does not enhance the conversion of glycerol as demonstrated by a glycerol conversion of 91.44% over 0.7KF/La-Zr. The results suggest the amount of KF is crucial for glycerol conversion to afford GC. The effects of the catalyst amount were also performed to obtain the optimal catalyst loading. Similarly, the glycerol conversion increases upon increasing the catalyst loading and reaches 91.51% at a catalyst loading of 1 wt.% of. More catalyst does not increase the glycerol conversion considerably as indicated by the glycerol conversion of 92.61% at a catalyst loading of 5 wt.%. Considering the significant dependence of the reaction on temperature, the effects of the reaction temperature were also investigated. The glycerol conversion increases from 36.30 to 91.51% upon increasing the reaction temperature from 70 to 80 ^{o}C. A further increase in temperature did not significantly enhance the conversion of glycerol. Thus, 80 ^{o}C was determined to be suitable for the reaction. According to the literature, a longer reaction time is beneficial for the transesterification of glycerol to give GC. The conversion of glycerol enhanced from 47.55 to 91.77% when the

reaction time was increased from 20 min to 60 min, and then remained almost unchanged upon further increasing the reaction time. Therefore, 60 min was determined as the optimal reaction time. In summary, the optimal reaction conditions are 0.3KF/La-Zr, 1 wt.% catalyst l, 80 ^{o}C and 60 min.

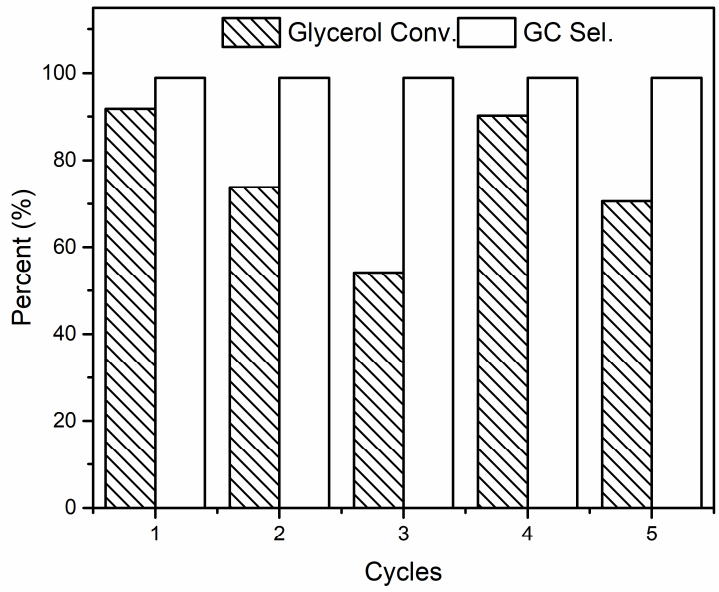

Fig. 8 Reusability of 0.3KF/La-Zr in the synthesis of GC. Reaction conditions: Glycerol 50 mmol, DMC 100 mmol, catalyst 1 wt.%, 80 ^{o}C, 60 min.

3. 3 Reusability of the catalyst

Reusability is the main criterion used to assess heterogeneous catalysts. The reuseability of 0.3KF/La-Zr is displayed in Fig. 8. The catalyst was recovered using simple filtration and calcination at 500 ^{o}C for 5 h to remove the adsorbed organic compounds, and then used for the next run. Clearly, the activity of 0.3KF/La-Zr for glycerol transesterification decreases upon increasing the cycle number. In the second cycle, the conversion of glycerol drops from 91.77 to 73.83%, and in the third run to 54.14%, suggesting the gradually deactivation of the catalyst. However, the selectivity of GC was almost unchanged during this process. The observed deactivation for glycerol conversion was mainly attributed to the loss of the strong and super basic sites, which results from the leaching of KF. KF can serve as a catalyst for GC decarbonylation to

afford GD at high temperature, as proved by the high selectivity of GD on gas chromatography. This means the KF leaching into the reaction solution during the reaction process was occurring. Considering the stability of the support, the catalyst was regenerated by reloading KF on the recovered support followed by calcination at 500 ^{o}C for 5 h. After this regeneration step, the catalyst exhibited a glycerol conversion of 90.18% and GC selectivity of 99% in the fourth cycle, suggesting the catalyst can be easily regenerated by reloading KF onto the recovered support.

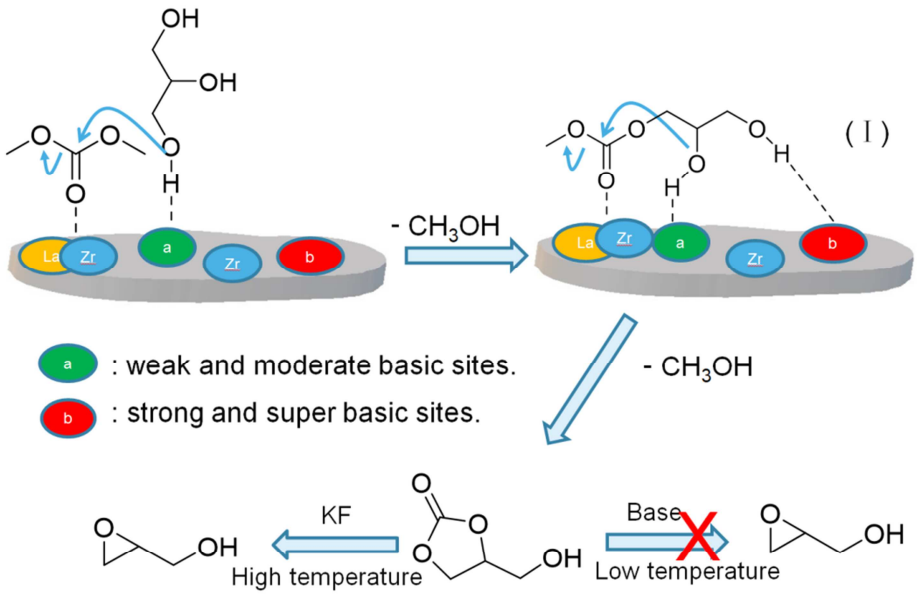

Fig. 9 Plausible reaction mechanism for synthesis of GC and GD from glycerol.

3.4 Reaction mechanism

The reaction of glycerol with dimethyl carbonate to afford GD involves two steps, as shown in Scheme 1. The first step can be easily achieved in the presence of a basic catalyst. However, the decarbonylation of GC is rather difficult. Based on the experimental and characterization results, the strong and super basic sites play a critical role in the first step, however, temperature seems to be the decisive factor in the second step. By combining the literature precedent [24, 28, 48] and our experimental and characterization results, a plausible reaction mechanism was proposed and displayed in Fig. 9. Firstly, the hydroxyl groups of glycerol are adsorbed and activated by the basic sites of the catalyst through hydrogen bonding. Meanwhile, dimethyl carbonate is activated by the Lewis acid sites (Zr^{4+}) in the catalyst. Thereafter, the activated hydroxyl groups undergo

nucleophilic attack on the carbonyl group of dimethyl carbonate, accompanied by the elimination of one molecule of methanol to give intermediate (I). Then, the activated hydroxyl groups and carbonyl groups of intermediate (I) undergo an intramolecular nucleophilic substitution along with the elimination of another molecule of methanol to give the product, GC. However, GC cannot be activated by the strong and super basic sites at low temperature to conduct a decarbonylation reaction to afford GD. However, at high temperature and in the presence of a metal salt, such as KF, GC can lose one molecule of CO_2 to give GD.

Conclusions

A series of novel catalysts were developed by loading KF onto a porous La-Zr-600 solid support and their catalytic performance investigated for glycerol conversion to prepare GC and GD. The characterization results showed that large number of weak, strong and super basic sites were generated upon loading KF on the La-Zr support. The weak basic sites were proposed to be associated with the Brønsted base generated during the reaction between KF and the La-Zr-600 support, while the strong and super basic sites were assigned to the Lewis base originating from the interaction between KF and the La-Zr-600 support. The high activity of the catalyst was related to the large number of strong and super basic sites generated on the catalyst's surface. The large amount of GD detected by gas chromatograph was attributed to the decomposition of GC due to the high temperature of the injection port. It was found that the strong and super basic sites play a key role in the transesterification of glycerol, while high temperature seems to be essential for the decarbonylation of GC to give GD. Finally, the catalyst can be easily regenerated by simply reloading KF onto the recovered catalyst.

Acknowledgments

This work was financially supported by National Natural Science Foundation of China (No. 21276050, 21676054 and 21406034), Natural Science foundation of Jiangsu (No. BK20161415), Open Found of Jiangsu key laboratory (No. JSBEM21409). We thank International Science Editing (http://www.internationalscienceediting.com) for editing this manuscript.

References

[1] Y. Zheng, X. Chen, Y. Shen, Commodity chemicals derived from glycerol, an important biorefinery feedstock, Chem Rev. 110 (2010) 5253-5277.

[2] M. Pagliaro, R. Ciriminna, H. Kimura, M. Rossi, C. Della Pina, From glycerol to value-added products, Angew. Chem. Int. Ed. 46 (2007) 4434-4440.

[3] P.A.L. Lopes, A.J.S. Mascarenhas, L.A. Silva, Sonochemical synthesis of $Cd_{1-x}Zn_xS$ solid solutions for application in photocatalytic reforming of glycerol to produce hydrogen, J. Alloys Compd. 649 (2015) 332-336.

[4] J.R. Ochoa-Gómez, O. Gómez-Jiménez-Aberasturi, C. Ramírez-López, M. Belsué, A Brief Review on Industrial Alternatives for the Manufacturing of Glycerol Carbonate, a Green Chemical, Org. Process Res. Dev. 16 (2012) 389-399.

[5] A. Behr, J. Eilting, K. Irawadi, J. Leschinski, F. Lindner, Improved utilisation of renewable resources: New important derivatives of glycerol, Green Chem. 10 (2008) 13-30.

[6] A. Duval, L. Avérous, Cyclic Carbonates as Safe and Versatile Etherifying Reagents for the Functionalization of Lignins and Tannins, ACS Sustainable Chem. Eng. 5 (2017) 7334-7343.

[7] U. Chandrakala, R.B.N. Prasad, B.L.A. Prabhavathi Devi, Glycerol Valorization as Biofuel Additives by Employing a Carbon-Based Solid Acid Catalyst Derived from Glycerol, Ind. Eng. Chem. Res. 53 (2014) 16164-16169.

[8] C.H. Ahn, J.-D. Jeon, S.-Y. Kwak, Photoelectrochemical effects of hyperbranched polyglycerol in gel electrolytes on the performance of dye-sensitized solar cells, J. Ind. Eng. Chem. 18 (2012) 2184-2190.

[9] L. Soh, M.J. Eckelman, Green Solvents in Biomass Processing, ACS Sustainable Chem. Eng. 4 (2016) 5821-5837.

[10] D. Taton, A. Borgne, M. Sepulchre, N. Spassky, Synthesis of chiral and racemic functional polymers from glycidol and thioglycidol, Macromol. Chem. Phys. 195 (1994) 139-148.

[11] M. Ricciardi, F. Passarini, I. Vassura, A. Proto, C. Capacchione, R. Cucciniello, D. Cespi, Glycidol, a Valuable Substrate for the Synthesis of Monoalkyl Glyceryl Ethers: A Simplified Life Cycle Approach, ChemSusChem 10 (2017) 2291-2300.

[12] F.B. Gebretsadik, J. Ruiz-Martinez, P. Salagre, Y. Cesteros, Glycidol hydrogenolysis on a cheap mesoporous acid saponite supported Ni catalyst as alternative approach to 1,3-propanediol synthesis, Appl. Catal., A 538 (2017) 91-98.

[13] P. Panja, P. Das, K. Mandal, N.R. Jana, Hyperbranched Polyglycerol Grafting on the Surface of Silica-Coated Nanoparticles for High Colloidal Stability and Low Nonspecific Interaction, ACS Sustainable Chem. Eng. 5 (2017) 4879-4889.

[14] Z.I. Ishak, N.A. Sairi, Y. Alias, M.K.T. Aroua, R. Yusoff, Production of glycerol carbonate from glycerol with aid of ionic liquid as catalyst, Chem. Eng. J. 297 (2016) 128-138.

[15] Z. Liu, J. Wang, M. Kang, N. Yin, X. Wang, Y. Tan, Y. Zhu, Structure-activity correlations of $LiNO_3/Mg_4AlO_{5.5}$ catalysts for glycerol carbonate synthesis from glycerol and dimethyl carbonate, J. Ind. Eng. Chem. 21 (2015) 394-399.

[16] Y. Wu, X. Song, F. Cai, G. Xiao, Synthesis of glycerol carbonate from glycerol and diethyl carbonate over Ce-NiO catalyst: The role of multiphase Ni, J. Alloys Compd. 720 (2017) 360-368.

[17] J. Malkemus, V. Currier, Method for preparing glycidol, US2856413 (1958).

[18] J.W. Yoo, Z. Mouloungui, A. Gaset, Method for producing an epoxide, in particular of glycidol, US6316641 (2001).

[19] S. Yuichiro, S. Tomoaki, T. Hiroki, U. Mistsuru, M. Namba, Process for producing glycidol,

US7868192-B1 (2011).

[20] J.S. Choi, F.S.H. Simanjuntaka, J.Y. Oh, K.I. Lee, S.D. Lee, M. Cheong, H.S. Kim, H. Lee, Ionic-liquid-catalyzed decarboxylation of glycerol carbonate to glycidol, J. Catal. 297 (2013) 248-255.

[21] C.L. Bolívar-Diaz, V. Calvino-Casilda, F. Rubio-Marcos, J.F. Fernández, M.A. Bañares, New concepts for process intensification in the conversion of glycerol carbonate to glycidol, Appl. Catal., B 129 (2013) 575-579.

[22] S.M. Gade, M.K. Munshi, B.M. Chherawalla, V.H. Rane, A.A. Kelkar, Synthesis of glycidol from glycerol and dimethyl carbonate using ionic liquid as a catalyst, Catal. Commun. 27 (2012) 184-188.

[23] M.K. Munshi, S.M. Gade, V.H. Rane, A.A. Kelkar, Role of cation–anion cooperation in the selective synthesis of glycidol from glycerol using DABCO–DMC ionic liquid as catalyst, RSC Adv. 4 (2014) 32127-32133.

[24] G. Parameswaram, M. Srinivas, B. Hari Babu, P.S. Sai Prasad, N. Lingaiah, Transesterification of glycerol with dimethyl carbonate for the synthesis of glycerol carbonate over Mg/Zr/Sr mixed oxide base catalysts, Catal. Sci. Technol. 3 (2013) 3242-3249.

[25] Y.T. Algoufi, U.G. Akpan, M. Asif, B.H. Hameed, One-pot synthesis of glycidol from glycerol and dimethyl carbonate over KF/sepiolite catalyst, Appl. Catal., A 487 (2014) 181-188.

[26] X. Song, Y. Wu, F. Cai, D. Pan, G. Xiao, High-efficiency and low-cost Li/ZnO catalysts for synthesis of glycerol carbonate from glycerol transesterification: The role of Li and ZnO interaction, Appl. Catal., A 532 (2017) 77-85.

[27] J. Granados-Reyes, P. Salagre, Y. Cesteros, Effect of the preparation conditions on the catalytic activity of calcined Ca/Al-layered double hydroxides for the synthesis of glycerol carbonate, Appl. Catal., A 536 (2017) 9-17.

[28] S.E. Kondawar, C.R. Patil, C.V. Rode, Tandem Synthesis of Glycidol via Transesterification of Glycerol with DMC over Ba-Mixed Metal Oxide Catalysts, ACS Sustainable Chem. Eng. 5 (2016) 1763-1774.

[29] W. Jiang, X. Niu, F. Yuan, Y. Zhu, H. Fu, Preparation of KF–$La_2O_2CO_3$ solid base catalysts and their excellent catalytic activities for transesterification of tributyrin with methanol, Catal. Sci. Technol. 4 (2014) 2957-2968.

[30] R. Song, D. Tong, J. Tang, C. Hu, Effect of Composition on the Structure and Catalytic Properties of KF/Mg–La Solid Base Catalysts for Biodiesel Synthesis via Transesterification of Cottonseed Oil, Energy Fuels 25 (2011) 2679-2686.

[31] X. Niu, C. Xing, W. Jiang, Y. Dong, F. Yuan, Y. Zhu, Activity and stability of solid base KF/La_2O_3 catalysts for transesterification of tributyrin with methanol, React. Kinet. Mech. Catal. 109 (2013) 167-179.

[32] S. Lou, L. Jia, X. Guo, P. Wu, L. Gao, J. Wang, Preparation of diethylene glycol monomethyl ether monolaurate catalyzed by active carbon supported KF/CaO, Springerplus 4 (2015) 686-696.

[33] N. Liu, Z. Wu, M. Li, S. Li, Y. Li, R. Yu, L. Pan, Y. Liu, A novel strategy for constructing mesoporous solid superbase catalysts: bimetallic Al–La oxides supported on SBA-15 modified with KF, Catal. Sci. Technol. 7 (2017) 725-733.

[34] X. Song, Y. Wu, D. Pan, F. Cai, G. Xiao, Carbon nitride as efficient catalyst for chemical fixation of CO_2 into chloropropene carbonate: Promotion effect of Cl in epichlorohydrin, Mol. Catal. 436 (2017) 228-236.

[35] X. Niu, J. Gao, Q. Miao, M. Dong, G. Wang, W. Fan, Z. Qin, J. Wang, Influence of preparation method on the performance of Zn-containing HZSM-5 catalysts in methanol-to-aromatics,

Microporous Mesoporous Mater. 197 (2014) 252-261.

[36] Y. Ni, A. Sun, X. Wu, G. Hai, J. Hu, T. Li, G. Li, The preparation of nano-sized H[Zn, Al]ZSM-5 zeolite and its application in the aromatization of methanol, Microporous Mesoporous Mater. 143 (2011) 435-442.

[37] C.-y. Park, H. Nguyen-Phu, E.W. Shin, Glycerol carbonation with CO_2 and $La_2O_2CO_3$/ZnO catalysts prepared by two different methods: Preferred reaction route depending on crystalline structure, Mol. Catal. 435 (2017) 99-109.

[38] D. Pakhare, V. Schwartz, V. Abdelsayed, D. Haynes, D. Shekhawat, J. Poston, J. Spivey, Kinetic and mechanistic study of dry (CO_2) reforming of methane over Rh-substituted $La_2Zr_2O_7$ pyrochlores, J. Catal. 316 (2014) 78-92.

[39] J. Ni, L. Chen, J. Lin, M.K. Schreyer, Z. Wang, S. Kawi, High performance of Mg–La mixed oxides supported Ni catalysts for dry reforming of methane: The effect of crystal structure, Int. J. Hydrogen Energy 38 (2013) 13631-13642.

[40] H. Sun, Y. Ding, J. Duan, Q. Zhang, Z. Wang, H. Lou, X. Zheng, Transesterification of sunflower oil to biodiesel on ZrO_2 supported La_2O_3 catalyst, Bioresour Technol. 101 (2010) 953-958.

[41] Y. Gao, Y. Zhang, Y. Zhou, C. Zhang, H. Zhang, S. Zhao, J. Fang, M. Huang, X. Sheng, Synthesis of ordered mesoporous La_2O_3-ZrO_2 composites with encapsulated Pt NPs and the effect of La-dopping on catalytic activity, J. Colloid Interface Sci. 503 (2017) 178-185.

[42] H. Zhang, S. Hao, J. Lin, Influence of Li_2O-B_2O_3 glass on ionic migration and interfacial properties of $La_{2/3-x}Li_{3x}TiO_3$ solid electrolyte, J. Alloys Compd. 704 (2017) 109-116.

[43] S. Suga, S. Imada, T. Muro, T. Fukawa, T. Shishidouau, Y. Tokura, Y. Moritomo, T. Miyahara, La 4d and Mn core absorption magnetic circular dichroism, XPS and inverse photoemission spectroscopy of Lal-xSrxMnO_3, J. Electron. Spectrosc. Relat. Phenom. 78 (1996) 283-286.

[44] W.-J. Liu, F.-X. Zeng, H. Jiang, X.-S. Zhang, W.-W. Li, Composite Fe_2O_3 and ZrO_2/Al_2O_3 photocatalyst: Preparation, characterization, and studies on the photocatalytic activity and chemical stability, Chem. Eng. J. 180 (2012) 9-18.

[45] N.A. Merino, B.P. Barbero, P. Eloy, L.E. Cadús, La1−xCaxCoO_3 perovskite-type oxides: Identification of the surface oxygen species by XPS, Appl. Surf. Sci. 253 (2006) 1489-1493.

[46] W. Gu, J. Liu, M. Hu, F. Wang, Y. Song, $La_2O_2CO_3$ Encapsulated La_2O_3 Nanoparticles Supported on Carbon as Superior Electrocatalysts for Oxygen Reduction Reaction, ACS Appl. Mater. Interfaces 7 (2015) 26914-26922.

[47] H. Li, D. Gao, P. Gao, F. Wang, N. Zhao, F. Xiao, W. Wei, Y. Sun, The synthesis of glycerol carbonate from glycerol and CO_2 over $La_2O_2CO_3$–ZnO catalysts, Catal. Sci. Technol. 3 (2013) 2801-2809.

[48] D.J. Darensbourg, A.D. Yeung, Kinetics and thermodynamics of the decarboxylation of 1,2-glycerol carbonate to produce glycidol: computational insights, Green Chem. 16 (2014) 247-252.

1. Porous La-Zr solid base was prepared with P123 as soft template.

2. Abundant various basic sites were generated upon loading with KF on La-Zr support.

3. KF/La-Zr catalysts displayed good catalytic performance in the preparation of glycerol carbonate.

4. The high catalytic performance was related to the strong and super basic sites.